Classification: Biological/Physical Sciences -- Microbiology

The elastic basis for the shape of the Lyme disease spirochete

Christopher Dombrowski[1], Wanxi Kan[2], Md. Abdul Motaleb[3], Nyles W. Charon[3], Raymond E. Goldstein[1,4], and Charles W. Wolgemuth[2]

[1]*University of Arizona, Department of Physics, Tucson, AZ 85721*

[2]*University of Connecticut Health Center, Department of Cell Biology and Center for Cell Analysis and Modeling, Farmington, CT 06030-3505*

[3]*West Virginia University, Department of Microbiology, Immunology, and Cell Biology, Morgantown, WV 26506-9177*

[4]*University of Cambridge, Department of Applied Mathematics and Theoretical Physics, Cambridge, UK CB3 0WA*

Corresponding Author:

Charles W. Wolgemuth
Department of Cell Biology
University of Connecticut Health Center
263 Farmington Avenue
Farmington, CT 06030-3505
(860) 679-1655
cwolgemuth@uchc.edu

Text pages: 14
Figures: 3
Words in Abstract: 179

Total Characters: 32,737

Abstract

The mechanisms that determine bacterial shape are in many ways poorly understood. A prime example is the Lyme disease spirochete, *Borrelia burgdorferi*, which mechanically couples its motility organelles, helical flagella, to its rod-shaped cell body, producing a striking flat-wave morphology. A mathematical model is developed here that accounts for the elastic coupling of the flagella to the cell cylinder and shows that the flat-wave morphology is in fact a natural consequence of the geometrical and material properties of the components. Optical trapping experiments were used to measure directly the mechanical properties of these spirochetes. We find the Young's moduli of the periplasmic flagella and the cell cylinder to be 700 MPa and 0.1 MPa, respectively. These results imply relative stiffnesses of the two components which confirm the predictions of the model and show that the morphology of *B. burgdorferi* is completely determined by the elastic properties of the flagella and cell body. This approach is applicable to a variety of other structures in which the shape of the composite system is markedly different from that of the individual components.

\body

Introduction

Spirochetes constitute a unique group of motile bacteria, with some members being highly virulent in humans. While the flagella of these bacteria are structurally similar to those of other species, they are encased within the periplasmic space which lies between the cell wall complex (i.e., cell cylinder) and the outer membrane. Although spirochetes vary tremendously with respect to habitat, size, number of periplasmic flagella attached at each end, and their mechanics of swimming, DNA sequence analysis indicates that they all evolved from a primordial protospirochete (1-3). Depending on the species, the final shape of a spirochete is either helical or a flat wave. As in other bacteria, the flagella serve an obvious motile function as they are driven by rotary motors at their base – but in spirochetes these organelles rotate between the outer membrane and cell cylinder (3). Species such as *Spirochaeta aurantia* and *Treponema primitia* swim by a mechanism in which the flagella do not deform the cell cylinder and do not influence cell shape (4, 5). In contrast, in other species, such as *Leptospira interrogans* and *Borrelia burgdorferi*, they are also skeletal organelles; cells lacking flagella or with straight flagella have altered shapes, and these mutants are also non-motile (6-10). Moreover, several models of spirochete locomotion indicate that the skeletal function of the periplasmic flagella is essential for their motility (3, 6, 11-13).

The basis for spirochete shape remains elusive. In some spirochete species, genetic evidence indicates that the helical cell shape of the cell is associated with the cell wall and is independent of the periplasmic flagella (3, 6, 8-10, 14). However, in others the final shape of the entire cell is due to complex interactions between the cell

cylinder and the periplasmic flagella. Specifically, the Lyme disease spirochete *B. burgdorferi*, and possibly the syphilis spirochete *Treponema pallidum* (15), have flat-wave morphologies. *B. burgdorferi* has a periodically undulating, nearly planar shape (**Figure 1**a,b,e,f). Remarkably, cells lacking FlaB, the primary constituent of the left-handed flagellar filament, are rod-shaped (3, 7, 12, 16) (**Figure 1**c,g). Thus, the periplasmic flagella play a major role in creating the flat-wave morphology in this species. Because *T. pallidum* is unable to be continuously cultured in vitro, we know very little about the factors that influence its shape.

The morphology and motility of *B. burgdorferi* has been characterized in detail. High voltage electron microscopy (13) has been used to determine the typical cell dimensions: the cell cylinder radius (a = 0.17 μm), length (10-20 μm), wavelength (λ = 2.83 μm), and undulation amplitude (h = 0.78 μm) (12, 13). Attached subterminally to the ends of the cell are between 7 and 11 flagellar filaments with a diameter of 20-24 nm (13, 17). Each filament is connected to a rotary motor anchored in the inner membrane of the cell. Spirochete flagellar motors, including those of *B. burgdorferi*, are similar to the motors found in other bacterial species (18, 19). Rotation of the periplasmic flagella of *B. burgdorferi* induces travelling-wave deformations of the cell cylinder, which provide the thrust that drives the swimming of these bacteria (12). Periplasmic flagella that are not constrained by the cell cylinder are left-handed helical filaments with a helix radius R = 0.14 μm and pitch P = 1.48 μm (20) (**Figure 1**d,h). In situ, the periplasmic flagella shape is dramatically different, due to its interaction with the cell cylinder. Although the shape is still left-handed, the flagella are stretched with R = 0.19-0.20 μm, and with a helical pitch of P = 2.83 μm (note that P = cell's λ).

These observations suggest a model for the development of the flat-wave morphology in *B. burgdorferi*. Enclosing the flagella inside the periplasmic space causes an elastic deformation of the cell cylinder, which in turn exerts a force back onto

the periplasmic flagella, causing them to deform as well. To explore whether this conceptual picture is sufficient to explain the flat-wave morphology, we developed and tested a mathematical model that treats the cell cylinder and the periplasmic flagella as filamentary elastic objects, since the cell cylinder and the flagella are much longer than they are wide. This approximation assumes that the cross sections of the filaments do not change appreciably during deformation, which is typically valid for long, thin objects that bend on length scales much longer than their diameter.

Results and Discussion

Theoretical Model. The energy required to twist or bend a filamentary elastic object is determined by two elastic moduli, each determined by a material property such as the Young's modulus and the radius of the filament. We denote the bending moduli of the cell cylinder and periplasmic flagella as A_c and A_f, respectively, and their twisting moduli by C_c and C_f. For most materials, the ratio of the twisting to bending modulus is between 2/3 and 1 (21). The equilibrium shape of the composite system of cell cylinder and flagella is determined by force and moment balances which incorporate the twisting and bending energy of the cell cylinder and of the periplasmic flagella, with the constraint that the flagella reside at the radius of the cell cylinder. Our model assumes that the flagella are localized at one position about the circumference of the cell cylinder (i.e., we treat all the flagella as a single filament) and that they are free to slide. A complete description of the mathematical model is given in the **Online Supplemental Material**. A similar, but simpler, version of this model was used previously to describe the shape and dynamics of the *Leptospiraceae* (22).

We treat the cell cylinder as a filament which, if isolated, would be straight, and the periplasmic flagella as a filament whose configuration in isolation would be a helix of radius R and pitch P, given above. We also assume that $C_f/A_f = C_c/A_c = 1$. Thus,

there are only two free parameters in the model, the radius *a* of the cell cylinder and the ratio $A = A_f/A_c$; these were varied to determine the range of shapes predicted by the model. When the cell cylinder is much stiffer than the flagella, the cell is nearly straight and the flagella wrap about it with a pitch that is larger than *P*. As the ratio A increases, the cell cylinder deforms into a flat-wave shape whose deformation amplitude increases while the wavelength decreases (**Figure 2**a,b). In this flat-wave shape, the model predicts that the periplasmic flagella should wrap about the cell cylinder in the opposite sense of their own handedness; i.e., a left-handed flagellum should wrap about the cell cylinder in a right-handed fashion, which agrees with previous experimental measurements (13). For values of A larger than 1.0, there is a noticeable axial rotation of the flat-wave morphology (**Figure 2**a), a precession about the cell axis that is often observed (12). The extent of precession depends on the relative positions of flagellar attachment points at the two ends. The amplitude of the morphology matches well with the experimental observations when $A > 3$. For values of $A < 5$, the wavelength that we calculate from the model is somewhat less than what is observed experimentally and does not depend strongly on the value of A (**Figure 2**b). Variation of the attachment positions of the flagella can increase or decrease the wavelength by roughly 10%. For $A > 5$, the wavelength approaches the pitch of the periplasmic flagella. Thus the model implies that the ratio A is approximately 3 - 5. We also found that the shape of the cell did not depend strongly on the values of the twisting moduli (results not shown).

The flat-wave shape of *B. burgdorferi* is thus due to a matching between the helical radius and pitch of the flagella and the radius of the cell cylinder. Our mathematical model suggests that the flat wave shape arises when the radius of the cell, *a*, is roughly equal to the helix radius of the flagellum times the square of the ratio of the length of one turn of the flagellum to the pitch: $a \sim R\,(4\pi^2R^2 + P^2)/P^2$. For *B. burgdorferi*, this implies that *a* is approximately 0.19 μm. When the cell cylinder's

radius is much smaller than that of the flagella, the cell is also helical (**Figure 2**c). Increasing the radius of the cell leads to a flatter morphology (**Figure 2**c).

Measurement of the elastic parameters confirms the model. To test the mathematical model, we measured the stiffness of the cell cylinder and the periplasmic flagella using optical trapping methods. For studies of the cell cylinder, detergent was used to remove the outer membrane of cells of *B. burgdorferi senso stricto* strain B31A, which exposes the cell wall. With the outer membrane removed, the flagella often remain intertwined about the cell cylinder. Polylysine-coated silica beads (1 μm diameter) were then attached to two points along the length of the cell. One of the beads was then anchored to a coverslip by attachment to another bead (**Figure 3**a). The second bead was positioned in an optical trap. A quadrant photodiode was used to measure and align the position of the bead in the optical trap as well as to calibrate the spring constant of the trap; all calibrations were done in Metamorph using video tracking of trapped beads imaged with very short (1 ms) shutter speeds (23). The microscope stage was oscillated and the displacement of the trapped bead with respect to the position of beads affixed to the coverslip was measured. Using this procedure, the force required to stretch the cells was determined (**Figure 3**b). The shape of *B. burgdorferi* is roughly sinusoidal (12, 13), and the force-displacement curves are well-fit by assuming that the cell behaves like an elastic sine wave (See **Online Supplemental Material** for more details). The effective bending modulus found using this fitting procedure is 42 ± 24 pN μm^2. By stretching the cell, bent regions where the periplasmic flagella are still wrapped about the cell body are straightened. Therefore, this bending modulus accounts for the combined effect of the cell cylinder and the periplasmic flagella. Our mathematical model predicts that the bending modulus that is measured by this experiment is $A_c + 0.6A_f$ (see **Online Supplemental Material**).

Using a similar experimental procedure, we also measured the stiffness of the purified periplasmic flagella. **Figure 3**c shows four representative force-displacement curves. We fit these data to theoretical curves generated numerically for stretching and compressing an elastic helix. From these fits, the bending modulus for the periplasmic flagellum was estimated to be 6.7 ± 3.7 pN μm^2. This value is of the same order as measurements of the bending modulus of flagellar filaments from *Salmonella enterica* serovar Typhimurium performed using quasi-elastic scattering of light (24) and extensional flow (25, 26). Using a flagellar diameter of 10 nm, we estimate the Young's modulus of the flagellum to be 700 MPa. Therefore, if there are 8 periplasmic flagella along the length of *B. burgdorferi*, A_f would be approximately 53 pN μm^2. From this result and the results from the cell stretching experiments, we estimate the bending modulus of the cell cylinder to be about 10 pN μm^2, which implies that $A \approx 5$, in good agreement with the results from the mathematical model. For an elastic tube, such as the cell wall, the Young's modulus, E, is related to the bending modulus as $A \sim \pi E a^3 t$. Here t is the thickness of the cell wall, which we estimate to be about 6nm. Therefore, the Young's modulus of the cell wall of *B. burgdorferi* is about 0.1 MPa, which is comparable to that measured for *Magnetospirillum gryphiswaldense* (27) and *Myxococcus xanthus* (28) but substantially lower than what has been estimated for *Escherichia coli* and *Bacillus subtilis* (29, 30).

We have shown that the mechanical coupling of the helical periplasmic flagella to the rod-shaped cell cylinder is sufficient to determine the flat-wave morphology of *B. burgdorferi*. In addition, we have measured the elastic parameters of both of these structures. In spirochetes, because the interaction between the PFs and cell cylinder is quite intimate, these organelles may have co-evolved to achieve optimal motility and for survival in nature. It is not clear why some spirochete species are helical, and others are flat waves. However, there are two obvious advantages to being a spirochete. First, all known spirochetes can swim efficiently in highly viscous gel-like media that slow down

or stop other species of bacteria (3, 31, 32). Second, because the periplasmic flagella are intracellular, these organelles are protected from harsh environments including specific antibodies (3). Evidently, each species evolved in a manner that maintained these attributes in order to best adapt to its specific ecological niche.

If the shape and dynamics of *B. burgdorferi* have evolved to allow for optimal motility and/or the ability to invade host tissue, then it is interesting to speculate about the physical consequences of our findings. Our results suggest that there are two major factors that can be adjusted to modify *B. burgdorferi*'s cell morphology, the geometric parameters of the helical flagella and the ratio of the stiffness of the periplasmic flagella to that of the cell cylinder. We find that the stiffness of an individual flagellum of *B. burgdorferi* is comparable to the stiffness that has been measured in other species, such as *Salmonella enterica* serovar Typhimurium (24-26). Therefore, it may be that bacterial flagellar stiffness is not evolutionarily tunable. However, some bacterial flagella have a sheath around the flagellum or have glycosylated or sulfated residues on the flagellum, which could be a method for increasing flagellar stiffness, but the stiffness of these flagella have not yet been measured (33-37).

The other ways that a spirochete could modify the stiffness ratio would be to alter the number of the flagella or the stiffness of the cell cylinder. Indeed, bacterial cell wall stiffness varies dramatically between bacterial species, as does the number of periplasmic flagella in spirochetes. Comparison of our measurements of the stiffness of the *B. burgdorferi* cell cylinder to theoretical estimates for *Leptonema illini* suggests that *B. burgdorferi*'s cell cylinder is considerably less stiff than that of *L. illini* (22).

Because the stiffness of a group of periplasmic flagella should increase with the number of filaments, this is another parameter that can be varied between species. If this line of reasoning is correct, then an individual spirochete could adjust its number of flagella in response to physical parameters of the environment in order to optimize its motility. Although other explanations are possible, this hypothesis could explain why in vitro culturing of *Borrelia garinii* results in a decreased number of periplasmic flagella and decreased motility in gel-like media (38). In fact, the flagella could even act as the regulatory sensor. In *Vibrio parahaemolyticus*, the polar flagellum acts as a mechanosensor that is sensitive to fluid viscosity and triggers lateral flagella synthesis for efficient swimming in highly viscous environments and on surfaces (35, 39).

Morphology of *B. burgdorferi* is implicitly connected with motility. Moreover, motility is likely to be essential for these organisms to cause disease (3, 38, 40). How rotation of the flagella produces the undulating motions that drive motility and enables translocation through host tissues remains unknown. However, the description of the physical interaction between the flagella and the cell cylinder developed here provides a basis for a quantitative model of the mechanism of motility in *B. burgdorferi* and will likely serve as a foundation for eventually understanding the motility of *T. pallidum*.

Many biological structures are composed of interconnected filamentary objects. At the single protein level, α helices often intertwine into helix bundles, such as the coiled-coil structure (41), and many receptor and motor proteins have large coiled-coil domains. At the molecular level, DNA, F-actin, microtubules, and the bacterial flagellum are all composed of multiple connected polymer strands or protofilaments. And, at the cellular level, the axoneme, which is the primary component of eukaryotic cilia and flagella, is composed of a cylindrical array of 9 microtubule doublets, crosslinked by dynein motors (42, 43). The mathematical model that is presented here

describes the complex physics of conjoined elastic filaments and should therefore be applicable to many of these structures. Indeed, simplified models have already been used to describe the dynamics of cilia (44), the configuration of the bacterial flagellum (45), and the structure of alpha-helical bundle proteins (46, 47).

Methods

Mathematical Model and Data Fitting

A complete description of the mathematical model and the method that we used to compute the elastic parameters from our data is given in the **Online Supplemental Material**.

Bacterial Strains

We used the high-passage *B. burgdorferi senso stricto* strain B31A, which has been previously described (7, 48).

Cell Cylinder Preparation

To remove the outer membrane of cells for use with the optical trapping experiments, we centrigued 25 ml of *B. burgdorferi senso stricto* strain B31A at 6000 X g for 20 min. The cells were then washed in 20 ml of 150 mM phosphate buffered saline, pH 7.4 (PBS) and then centrifuged again at 6000 X g for 15 min. We resuspended the pellet in 10 ml of PBS with myristate detergent (final concentration 1%), and the solution was shaken in a 37^{o} C water bath for 12 minutes and then centrifuged at 6000 X g for 15 min, washed, and re-centrifuged at 6000 X g for 15 minutes. Finally, the pellet was resuspended in 2-3 ml of water and a pipette was used to disperse the cells.

Measurement of the Cellular Morphology

Darkfield images of *B. burgdorferi* strain B31A with and without the outer membrane were taken using a Zeiss Axioscope 2 (100 X oil immersion objective) connected to a Hamamatsu digital camera (C4742-95). The peak-to-peak amplitude and wavelength were measured using the ``Line tool" in Volocity 4 software (Improvision Inc., Coventry, UK). At least 8-12 individual cells were measured.

Purification of the Periplasmic Flagella

Periplasmic flagella were purified using a method similar to that given in (18). Approximately 250 ml of late logarithmic phase cells (1 X 10^8 cells/ml) were centrifuged at 6000 X g for 20 minutes (all centrifuation was done at 4^o C). The pellet was washed in 30 ml of sucrose solution (0.5M sucrose, 0.15M Tris-HCl, pH 8) and re centrifuged at 6000 X g for 15 minutes. The pellet was then resuspended in 15 ml sucrose solution and stirred on ice for 10 minutes, 0.15 ml of lysozyme (10 mg/ml) was slowly added, and then the solution was stirred on ice for 5 minutes. 1.5 ml EDTA (stock 20 mM) was added to a final concentration of 2 mM and the solution was then stirred on ice for 20 min, and then stirred at room temperature for 40 min. Approximately 1.5 ml myristate detergent (stock 10% in PBS) was added to a final concentration of 1%, and then it was stirred at room temperature for 1 hour. 0.3 ml $MgSO_4$ (stock 0.1M) was added and then the solution was stirred at room temperature for 5 min. 0.3 ml EDTA (stock 0.1M) was added, then the solution was stirred for 5 min and centrifuged at 17,000 X g for 15 min. The soup was taken and 2 ml PEG solution (stock 20% PEG in 1M NaCl) was added, and then it was put on ice for 30 min. The solution was centrifuged at 27,000 X g for 20 min. The pellet was resuspended in 5 ml

H_2O and then recentrifuged at 85,000 X g for 30 min, and the pellet was resuspended in 1 ml H_2O and stored at 4^oC.

Coverslip Preparation

2 μm diameter polystyrene spheres were coated with poly-L-lysine and placed in a 100 mM NaCl solution. The 2 μm spheres were then flowed into a flowcell and let stand for approximately 10 minutes to allow them to settle and stick to the surface of the coverslip to provide reference points and spacers in the experiment. The fluid was then exchanged with dionized H_2O (ddH_2O) to remove excess, non-stuck, spheres from the flowcell. The experimental assay was then flowed into the chamber.

Optical Trapping Experiments

The flagellar assay consisted of a dilution of purified flagella from *B. burgdorferi* and 1 μm silica spheres coated with poly-L-lysine in 0.6% methylcellulose solution with 100mM NaCl.

The cell cylinder assay consisted of a dilution of spirochete cell cylinders and 1 μm silica spheres coated with poly-L-lysine in 0.6% methylcellulose solution with 50 mM NaCl added. The solution was pH adjusted to 7.5-8.9 using $NaHCO_3$.

For individual flagellum measurements, the sample was searched for bead flagellum pairs with one end of the flagellum spontaneously adherent to the surface. The tethered bead was trapped and brought to a height of 0.76 μm off the surface of the coverslip. In the case of surface tethered flagella, the *y* position was adjusted in order to triangulate the point of attachment and determine the length of the flagella.

For cell cylinder measurements, cells were found that had a 1 μm sphere attached somewhere along the length. This sphere was attached to the surface. A second bead was attached to the distal end of the cell and was brought to a known height off the surface of the coverslip.

The piezo stage (MadCity Labs, Nano-H100) was driven with a triangle wave (Agilent 33220A). The *y* position of the stage was adjusted such that the stretching of the flagella or cell was purely in the *x* direction. The amplitude, frequency, and offset position of the stage were adjusted so that the stretching event occurred at an appropriate rate for tracking and to ensure that the event included the unstressed configuration of the cell or flagellum (nominally 50-100 mV, @ 0.25 Hz).

A quadrant photodiode (QPD) was used to image the trapped bead in the back focal plane of the condenser and was used to monitor and adjust the position of the bead in the trap. Trap calibration was done by taking 10 sets of 500 images of the trapped bead (at a specified height) with a 1ms physical shutter for calibration of the trap (Photometrics, Quantex 57). This exposure time was necessary to match the characteristic time of a bead in the trap and minimize overestimation of the trap stiffness. The calibration images were reduced to remove optical and electronic noise (49) using Image J (NIH). The positions of the beads were then tracked using ``Track Particles" in Metamorph (Molecular Devices) following the guidelines set out by Carter, et al. (50). The bead tracks were then used to calibrate the trap stiffness, *K*, using the equipartition method (23).

The stiffness *K* was calculated for each bead in the calibration set and averaged. The weighted average of all of the beads was then calculated giving the average trap

stiffness. In the case of surface stretching experiments where the ``test" bead could not be calibrated directly, the optical trap stiffness was determined by the weighted average of all the *K* values for a given height in a given experiment (n ~ 10).

The stretching angle in *z* was taken into account for determining the cell/flagellum lengths and in the force calculations.

Acknowledgements. We thank S.F. Goldstein for discussions and the image shown in Figure 1d. This research was supported by the NIH (R01GM072004). CW thanks the Aspen Center for Physics where some of this work was completed.

Supplemental Material accompanies this paper on *PNAS*'s website (http://www.pnas.org).

Correspondence and requests for materials should be addressed to C. Wolgemuth (e-mail: cwolgemuth@uchc.edu).

References

1. Paster, B. J. & Dewhirst, F. E. (2000) *J. Mol. Microbiol. Biotechnol.* **2,** 341-344.

2. Canale-Parola, E. (1984) in *Bergey's manual of systematic biology.*, eds. Krieg, N. R. & Holt, J. G. (Williams and Wilkins, Baltimore, MD).

3. Charon, N. W. & Goldstein, S. F. (2002) *Annu. Rev. Genet.* **36,** 47-73.

4. Berg, H. C. (1976) *J. Theor. Biol.* **56,** 269-273.

5. Murphy, G. E., Matson, E. G., Leadbetter, J. R., Berg, H. C. & Jensen, G. J. (2008) *Mol. Microbiol.* **67,** 1184-1195.

6. Charon, N. W., Goldstein, S. F., Curci, K. & Limberger, R. J. (1991) *J. Bacteriol.* **173,** 4820-4826.

7. Motaleb, M. A., Corum, L., Bono, J. L., Elias, A. F., Rosa, P., Samuels, D. S. & Charon, N. W. (2000) *Proc. Natl. Acad. Sci. USA* **97,** 10899-10904.

8. Ruby, J. D., Li, H., Kuramitsu, H., Norris, S. J., Goldstein, S. F., Buttle, K. F. & Charon, N. W. (1997) *J. Bacteriol.* **179,** 1628-1635.

9. Bromley, D. B. & Charon, N. W. (1979) *J. Bacteriol.* **137,** 1406-1412.

10. Picardeau, M., Brenot, A. & Saint, I. (2001) *Mol. Microbiol.* **40,** 189-199.

11. Berg, H. C., Bromley, D. B. & Charon, N. W. (1978) in *Symp. Soc. Gen. Microbiol.*, Vol. 28, pp. 285-294.

12. Goldstein, S. F., Charon, N. W. & Kreiling, J. A. (1994) *Proc. Natl. Acad. Sci. USA* **91,** 3433-3437.

13. Goldstein, S. F., Buttle, K. F. & Charon, N. W. (1996) *J. Bacteriol.* **178,** 6539-6545.

14. Wolgemuth, C. W., Charon, N. W., Goldstein, S. F. & Goldstein, R. E. (2006) *J. Mol. Microbiol. Biotechnol.* **11,** 221-227.

15. Cox, C. D. (1972) *J. Bacteriol.* **109,** 943-944.

16. Sartakova, M. L., Dobrikova, E. Y., Motaleb, M. A., Godfrey, H. P., Charon, N. W. & Cabello, F. C. (2001) *J. Bacteriol.* **183,** 6558-6564.

17. Hovind Hougen, K. (1984) *Yale J. Biol. Med.* **57,** 543-548.

18. Sal, M. S., Motaleb, M. A., Shibata, S., Aizawa, S. I. & Charon, N. W. (2008) *J. Bacteriol.* **190,** 1912-1921.

19. Murphy, G. E., Leadbetter, J. R. & Jensen, G. J. (2006) *Nature* **442,** 1062-1064.

20. Charon, N. W., Goldstein, S. F., Block, S. M., Curci, K. & Ruby, J. D. (1992) *J. Bacteriol.* **174,** 832-840.

21. Landau, L. D. & Lifshitz, E. M. (1986) *Theory of Elasticity* (Butterworth-Heinenann Ltd., Oxford).

22. Kan, W. & Wolgemuth, C. W. (2006) *Biophys. J.* **93,** 54-61.

23. Neuman, K. C. & Block, S. M. (2004) *Rev. Sci. Instrum.* **75,** 2787-2809.

24. Fujime, S., Maruyana, M. & Asakura, S. (1972) *J. Mol. Biol.* **68,** 347-359.

25. Hoshikawa, H. & Kamiya, R. (1985) *Biophys. Chem.* **22,** 159-166.

26. Kim, M. J. & Powers, T. R. (2005) *Phys. Rev. E* **71,** 021914.

27. Arnoldi, M., Fritz, M., Bauerlein, E., Radmacher, M., Sackmann, E. & Boulbitch, A. (2000) *Phys. Rev. E* **62,** 1034-1044.

28. Pelling, A. E., Li, Y., Shi, W. & Gimzewski, J. (2005) *Proc. Natl. Acad. Sci. USA* **102,** 6484-6489.

29. Thwaites, J. J. & Mendelson, N. H. (1991) *Adv. Microb. Physiol.* **32,** 173-222.

30. Mendelson, N. H., Sarlls, J. E., Wolgemuth, C. W. & Goldstein, R. E. (2000) *Phys. Rev. Lett.* **84,** 1627-1630.

31. Berg, H. C. & Turner, L. (1979) *Nature* **278,** 349-351.

32. Greenberg, E. P. & Canale-Parola, E. (1977) *J. Bacteriol.* **131,** 960-969.

33. Trachtenberg, S., DeRosier, D. J. & Macnab, R. M. (1987) *J. Mol. Biol.* **195,** 603-620.

34. Li, C., Wolgemuth, C. W., Marko, M., Morgan, D. G. & Charon, N. W. (2008) *J. Bacteriol.***,** (in press).

35. McCarter, L. L. (2001) *Microbiol. Mol. Biol. Rev.* **65,** 445-462.

36. Taguchi, F., Shibata, S., Suzuki, T., Ogawa, Y., Aizawa, S.-I., Takeuchi, K. & Ichinose, Y. (2008) *J. Bacteriol.* **190,** 764-768.

37. Logan, S. M. (2006) *Microbiol.* **152,** 1249-1262.

38. Sellek, R. E., Escudero, R., Gil, H., Rodriquez, I., Chaparro, E., Perez-Pastrana, E., Vivo, A. & Anda, P. (2002) *Infect. Immun.* **70,** 4851-4858.

39. Belas, R., Simon, M. & Silverman, M. (1986) *J. Bacteriol.* **167,** 210-218.

40. Botkin, D. J., Abbott, A. N., Stewart, P. E., Rosa, P. A., Kawabata, H., Watanabe, H. & Norris, S. J. (2006) *Infect. Immun.* **74,** 6690-6699.

41. Lupas, A. (1996) *Trends Biochem. Sci.* **21,** 375-382.

42. Afzelius, B. A., Dallai, R., Lanzavecchia, S. & Bellon, P. L. (1995) *Tissue Cell* **27,** 241-247.

43. Nicastro, D., Schwartz, C., Pierson, J., Gaudette, R., Porter, M. E. & McIntosh, J. R. (2006) *Science* **313,** 944-948.

44. Hilfinger, A. & Julicher, F. (2008) *Phys. Biol.* **5,** 016003.

45. Srigiriraju, S. V. & Powers, T. R. (2005) *Phys. Rev. Lett.* **94,** 248101.

46. Wolgemuth, C. W. & Sun, S. X. (2006) *Phys. Rev. Lett.* **97,** 248101.

47. Neukirch, S., Goriely, A. & Hausrath, A. C. (2008) *Phys. Rev. Lett.* **100,** 038105.

48. Bono, J. L., Elias, A. F., III, J. J. K., Stevenson, B., Tilly, K. & Rosa, P. (2000) *J. Bacteriol.* **182,** 2445-2452.

49. Howell, S. B. (2000) *Handbook of CCD Astronomy.* (Cambridge University Press, Cambridge, UK).

50. Carter, B. C., Shubeita, G. T. & Gross, S. P. (2005) *Phys. Biol.* **2,** 60-72.

Figure Captions

Figure 1 The morphology and architecture of *B. burgdorferi*, which has a planar, flat-wave morphology. (a,e) When viewed from one perspective, the cell body appears wave-like; (b,f) When rotated by 90 degrees, the cell shape appears straight. (e,f) Schematic of the cell construction of *B. burgdorferi*. The cell cylinder is shown in green and the perplasmic flagellar bundle in purple. The outer membrane sheath is not shown. The flagella wrap around the cell body, inducing a flat-wave shape, with a wavelength of λ and amplitude *h*. The shapes shown here were produced by the mathematical model with parameters $a = 0.2$ μm and $A = 5$. (c) Mutants lacking FlaB do not produce flagella, and the cells are rod-shaped. Scale bar, 5 μm. Figure originally published in (3) and reproduced with permission. (g) Schematic of the cell cylinder. The radius of the cell cylinder is *a*. (d) Darkfield image of purified flagella from *B. burgdorferi*. Scale bar, 2 μm. Image courtesy of S. Goldstein. (h) Purified flagella are helical with a pitch, P and diameter 2R. (a,b) Scale bars,1 μm. Figures originally published in (12).

Figure 2 Predictions of the mathematical model. (a) Increasing the stiffness of the periplasmic flagella leads to larger deformations of the cell cylinder. For values of A between 1 and 5, the flat wave shape precesses about the long axis of the cell morphology, which leads to a non-planar waveform (bottom figure). (b) The model predicts that increasing the ratio A leads to a decrease in the wavelength of the cell cylinder deformation, λ (solid line), and an increase in the amplitude, *h* (dashed line). (c) Effect of changes in the cell radius. For small values of the cell radius, *a*, the shape of the cell is helical. As the cell radius increases, the shape becomes more flattened. Here values for *a* are given in microns.

Figure 3 Experimental measurement of the stiffness of the cell cylinder and the periplasmic flagella. (a) Schematic of the experimental setup. Polystyrene beads are attached to two points on the cell cylinder of Triton X treated cells or a purified flagellum. One of the beads is anchored to the coverslip via adhesion to another bead.

The other bead is trapped in an optical trap. Oscillation of the microscope stage deforms the cell cylinder or flagellum. A quadrant photodiode detector is used to measure displacement of the bead in the trap. Video images are used to measure the displacement of the trapped bead with respect to fixed beads on the surface of the coverslip. (b) Six representative plots of the force vs. displacement of the cell cylinder (See text and online Experimental Procedure). Different colors represent data from different experiments. The black lines show the fits to the data. (c) Four representative experiments for stretching purified flagella. Black circles are the experimental data. Solid lines show the fits to a model for deforming a linear elastic helix.

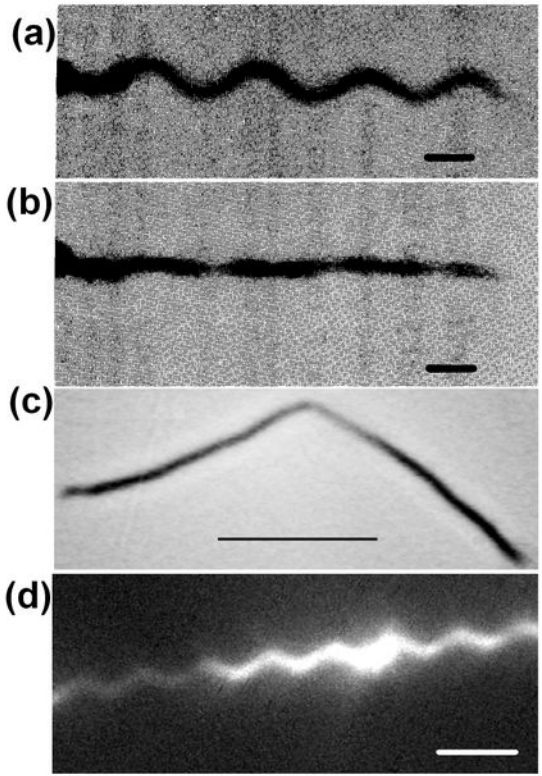
(a)
(b)
(c)
(d)

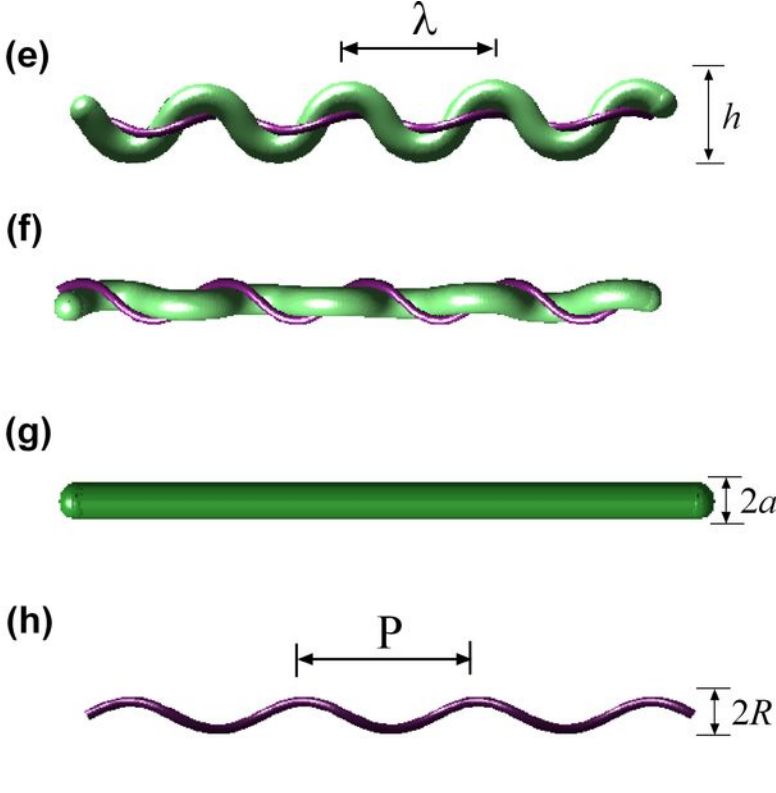
(e)
λ
h
(f)
(g)
2a
(h)
P
2R

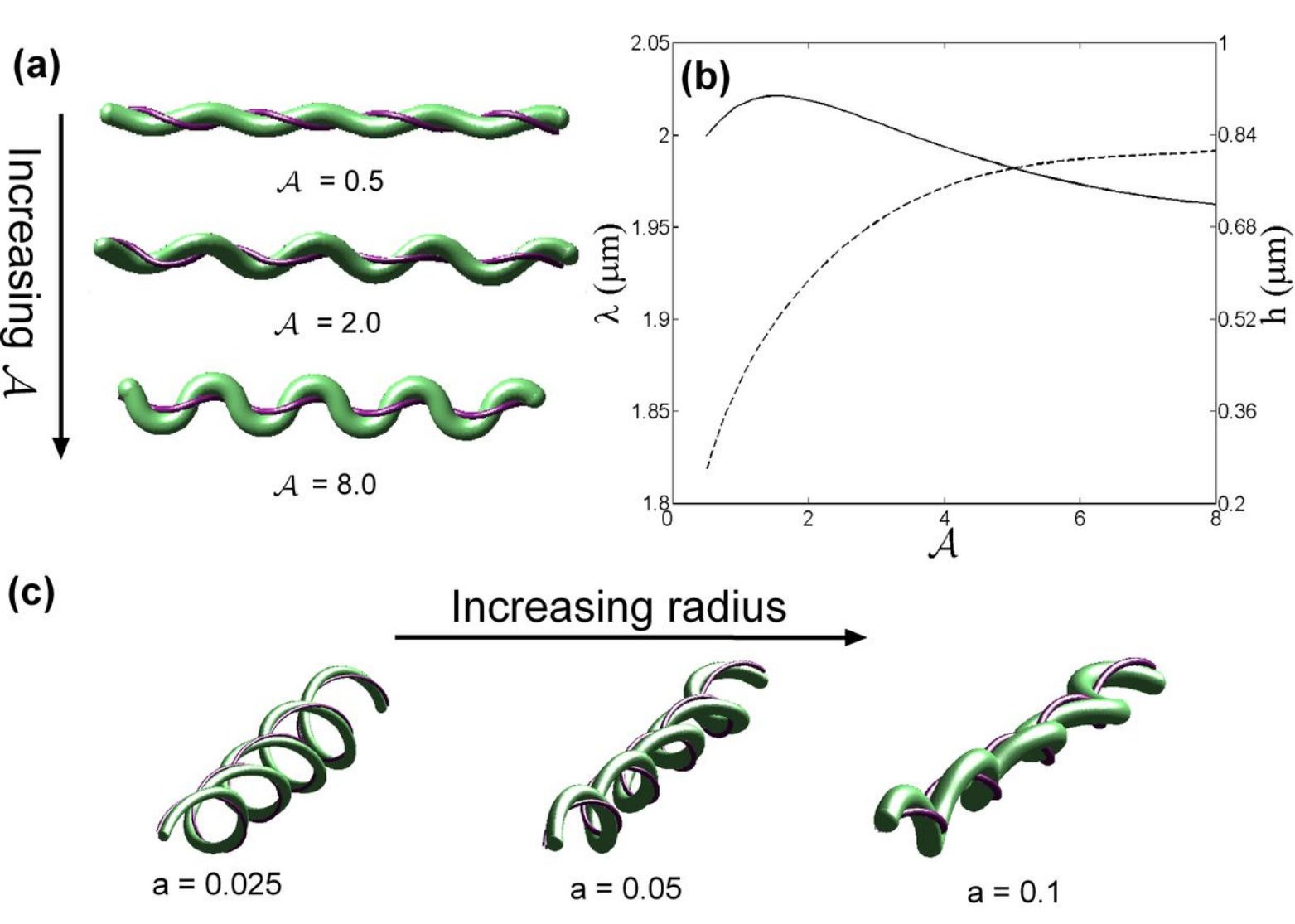
(a)
Increasing $\mathcal{A}$
$\mathcal{A}$ = 0.5
$\mathcal{A}$ = 2.0
$\mathcal{A}$ = 8.0
(b)
2.05
2
1.95
1.9
1.85
1.8
λ (μm)
1
0.84
0.68
0.52
0.36
0.2
h (μm)
0
2
4
6
8
$\mathcal{A}$
(c)
Increasing radius
a = 0.025
a = 0.05
a = 0.1

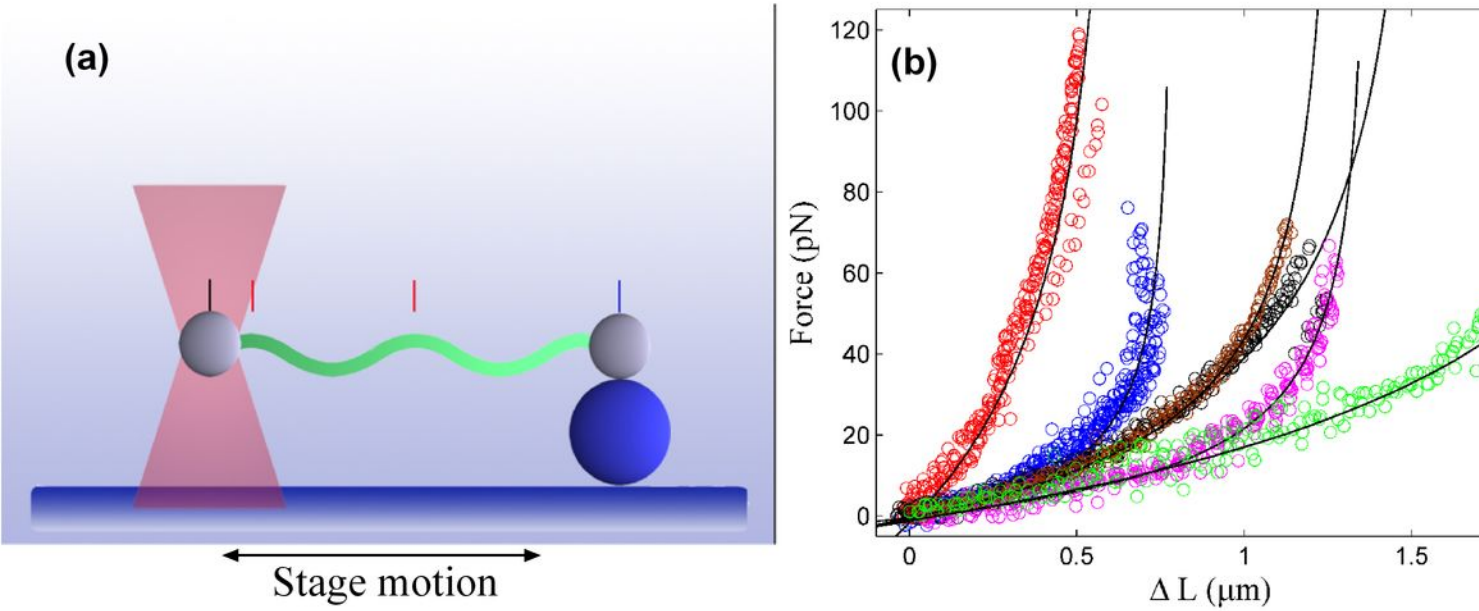
(a)
Stage motion
(b)
Force (pN)
Δ L (μm)

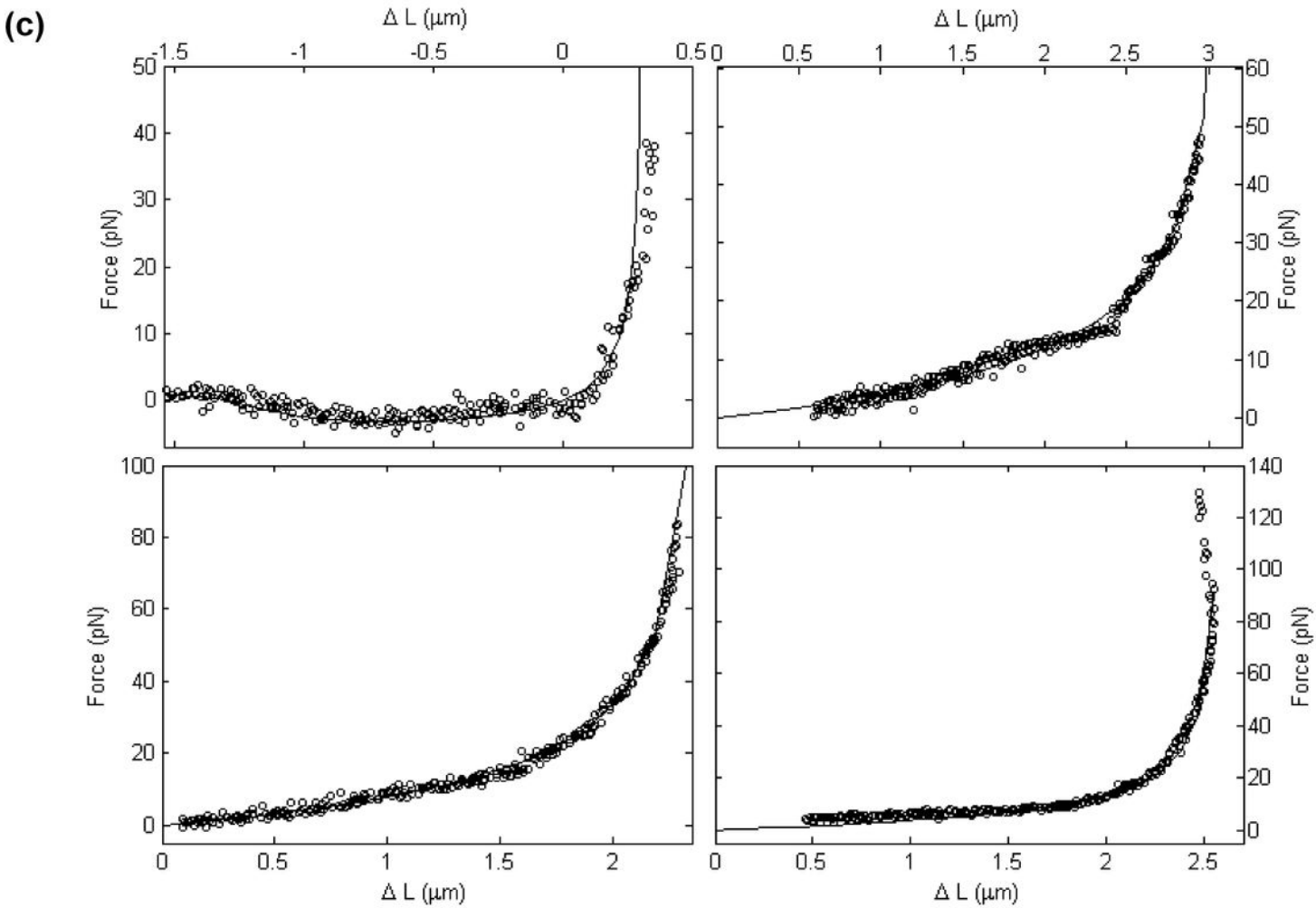
(c)
Δ L (μm)
Force (pN)